Supplemental Materials

Molecular Biology of the Cell

Nithianantham *et al.*

Figure S1. Details of the BASS-XL x-ray crystal structure determination.

A) Purification and Crystallization of the BASS-XL protein: left panel, Size Exclusion Chromatography (SEC) trace showing the purified BASS-XL. Middle panel, SDS-PAGE of purified BASS-XL. Right panel, images of BASS-XL C2 crystals used for x-ray structure determination.
B) Alignment of the BASS (grey) and BASS-XL (red) N-terminal structure ends to reveal the extension of the BASS-XL and the formation of the heptad repeats at the N-terminal end.
C) 2Fo-Fc map revealing the final model for BASS-XL built using the BASS-XL crystallographic data at 4.4-Å resolution. The model reveals the detailed helical coiled-coil dimers at the BASS-XL N-terminal end.
D) Crystallographic packing organization of BASS-XL minifilaments within the C2 space group for crystals used for structure determination.

Figure S2. Designing mini-tetramers using the BASS-XL x-ray structure.

A) Domain organization of designer *Drosophila* kinesin-5 mini-tetramers. KLP61F motor and neck linker domain (orange: residues 1-369) were fused to an extended BASS-XL minifilament, with its coiled-coil extension (green), dimerized region (cyan), tetrameric region (red) and C-terminal stabilizing zone (blue). The kMBXt construct included fusing the C-terminal kinesin-5 tail domain (residues 910-1036) to the C-terminal domain of the BASS-XL minifilament.
B) top panel, SEC-trace and SDS-PAGE for a peak fraction of the bacterially expressed C-terminally neon green (NG) tagged KMBX and kMBXt motors. Lower panel, mass photometry measurements for purified kMBX and KMBXt motors show assemblies with tetrameric oligomerization. Each panel shows fitted histograms of mass counts, based on a standard calibration. The theoretical tetrameric masses for each construct, shown on the lower left side of each panel, match the overall mass of the dominant species measured.
C) Top, a side view of a structural model revealing the organization of the designed bipolar mini-tetrameric kinesin-5 motor with various regions (colored as described A) shown. The model reveals the motor neck-linker domains are oriented to face in different directions due to their positioning on the BASS-XL minifilament and the mini-tetrameric motor is 38 nm in length, which is roughly half the length of native kinesin-5. Below, is a 90° rotated view of the view shown on top.
D) a subunit-colored view of the kinesin-5 mini-tetrameric motor design revealing the subunit organization of the motor and minifilament domains.

Figure S3: supporting single-molecule analyses of human kinesin-5 mini tetramers

A) Additional traces of parsing analysis for trajectories of hMBXt, similar to Figure 3A. Pauses (red) and periods of processive motility (blue) were identified in trajectories (top plots) based on the local α-value calculated within a sliding window along the trajectory, which fluctuated between ~2 and ~0 (bottom plots).
B) Histograms showing the number of distinct sections identified as paused for hMBXt motors (purple) and hMBX motors (green) in a given trajectory as a fraction of the number of long trajectories (n = 143 for hMBXt and n = 111 for hMBX).
C) the number of all trajectories >3 frames (n = 1406 for hMBXt motors and n = 2056 for hMBX). Few trajectories for hMBX motors were long enough to be used in our parsing analysis and, as short trajectories were less likely to contain pauses (see, for example, Figure 3C).
D, E) MSD curves for paused (red) and processive (blue) sections for hMBXt **(D)** and hMBX **(E)** motors plotted on a linear scale, revealing the parabolic shape characteristic of super-diffusive motility for processive sections, and a horizontal line for paused sections. Lines were fit to $\langle x^2\rangle=(v^2+\sigma_v^2)\tau^2+2\varepsilon^2$ and $\langle x^2\rangle=2\varepsilon^2$, respectively. Error bars represent SEM. For a, n = 143 trajectories from 9 independent experiments. For b, n = 111 trajectories from 3 independent experiments.

F) Kymograph showing the static binding of mini-tetramers in the presence of AMP-PNP. Scale bar 10s wide and 1μm tall.

G) Repeating the local-value analysis for mini-tetramers with the tail domain in the presence of AMP-PNP (black; dotted line) reveals a unimodal distribution, similar to the mean value of the paused sections (red; solid line) in the presence of ATP. In contrast, the mean α-value of processive sections (blue; solid line) in the presence of ATP is closer to 2. For AMP-PNP, n = 442 trajectories from 2 independent experiments. For ATP, n = 143 trajectories from 9 independent experiments.

Figure S4. **Measuring clustering and MT plus end residence using tracking and intensity analyses.**

A) Fluorescent Particle analyses: Right, Low magnification view of the MT (left) and kMBXt (right field) prior to analysis. Left, the intensity analysis (right) for all spots detected (left) was identified via the TrackMate plugin using FIJI/ImageJ. The kMBXt intensity histogram presented was converted into cluster values based on the fluorescence intensity of NG per motor subunit within each mini-tetramer. Details are described in materials and methods.

B) Example kymographs for kMBXt clusters at 25-150 mM KCl
Left to right, Example kymographs of kMBXt clustering along MTs at (A) 25 mM, (B) 50 mM, (C)100 mM, (D) 125 mM KCl, and (E) 150 mM KCl conditions. The kymographs show that clustering increases dramatically from 25 to 100 mM KCl, but it decreases at 125 and 150 mM KCl. The MT plus-end accumulation seems to concentrate the largest kMBX clusters (left side of each kymograph). Right panel, Description for types of cluster and motor merging events described in Figure 4 figure supplement 4B.

C, D, E, F) Characterizing kMBXt motility properties to cluster formation. Distribution for velocity (C), Run length. (D) and Run time (E) for kMBX (green) and kMBXt (purple) at 25-150 mM KCl. F) The types of clusters formed for kMBXt at different conditions. For each type, a smaller intensity spot merges with a larger intensity spot (i.e., 1+2). These intensities were delineated using the approach presented in B and described in materials and methods. G) Relationship of kMBXt velocity (left), Run length (middle) and run time(right) to cluster size for the 25 mM (green), 50 mM (pink), 100 mM (Gray), 125 mM (Cyan) and 150 mM KCl (orange). These data show that cluster size does not correlate to any of the properties described.

H, I, J, K, L) Analyses of MT plus-end accumulation of hMBX and HMBXt kinesin-5 mini-tetramers.

H) Clusters, which generally arrive at plus-ends as assemblies and dissociate as assemblies, were detected based on the intensity in a ROI over time. The blue line denotes the intensity trace in ROI at the plus-end of a MT. Magenta spots identify frames in which no motor is identified as present. Green spots identify frames in which the motor is identified as present. Other thin lines denote intensity traces of background ROIs used as a reference to identify the presence of a motor. Inset: An example of a motor arriving and falling off a plus-end is shown. 20 frames between time points. Scale bar 1μm wide.

I) Histograms of the frame-to-frame velocities for single motors (light purple; dotted line) and clusters (dark purple; solid line). During the processive sections of trajectories, clusters move more slowly than single motors. Their velocities during paused sections are similar. For a and e, n = 143 trajectories from 9 independent experiments for hMBXt and n = 111 trajectories from 3 independent experiments for hMBX. For b and c, n = 351 plus-end clusters detected from 8 independent experiments for hMBXt motors, and n = 211 plus-end clusters detected from 3 independent experiments for hMBX motors.

J) Traces of cluster detection at the plus-ends of MTs. Clusters generally arrive at plus-ends as a whole and dissociate, regardless of the plateau intensity, but we did observe single motors appearing to join a pre-existing cluster, as well as some clusters forming at the plus-end (e.g., top left). The blue

line denotes the intensity trace in ROI at the plus-end of an MT. Magenta spots identify frames in which no motor is identified as present. Green spots identify frames in which the motor is identified as present. Other thin lines denote intensity traces of background ROIs used as a reference to identify the presence of a motor. Left four traces for hMBXt motors and right two for hMBX motors.

K) An example of a cluster of human kinesin-5 HMBXt motors dragging the plus-end at which the motors accumulated along another MT, acting to align the two MTs. This demonstrates that the plus-end clusters are still motile and can withstand load (the MTs are quite bent and still anchored to the coverslip at some sites by an avidin-biotin interaction). Note that to observe this, a higher density of MTs was immobilized using a lower density of Neutravidin. 50 frames between time points. Scale bar 2μm wide.

Figure S5: Analyses of MT sliding trajectories for native and mini-tetramer kinesin-5: Individual frames from time-lapse image series were processed via linescan analysis to determine MT minus-end positions. These values are then plotted as a function of time for (a) hFLt and (b) kMBXt proteins. Velocities are calculated by applying a sliding window function of width 5 frames to the position data and a linear slope is calculated for the corresponding data sets (b,d). Velocity values below 15 nm/s for more than 3 consecutive frames were then classified as pausing events (red dashed line in b,d).

A **Purification and crystallization of BASS-XL protein**

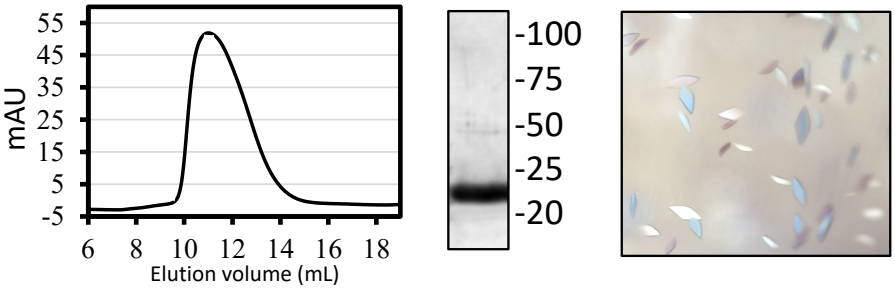

B **BASS-XL structure superimposed onto BASS structure (PDB ID: 4PXT)**

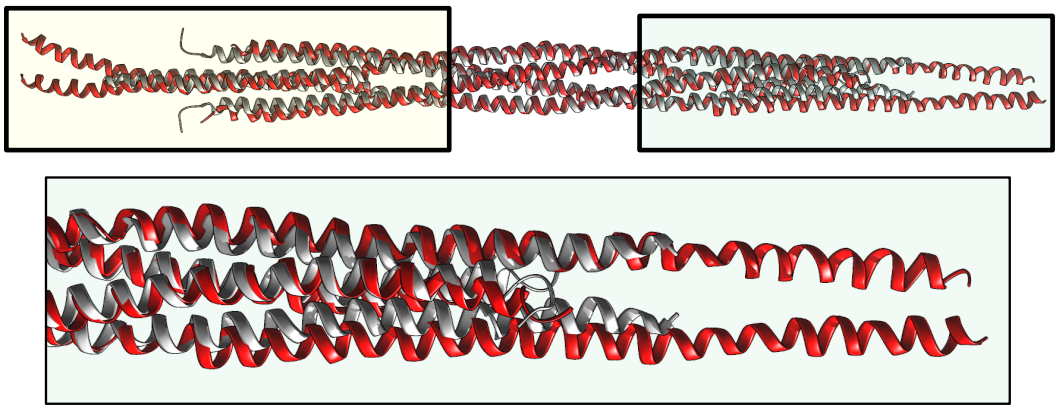

C **A Fourier (2Fo-Fc) electron density map of BASS-XL**

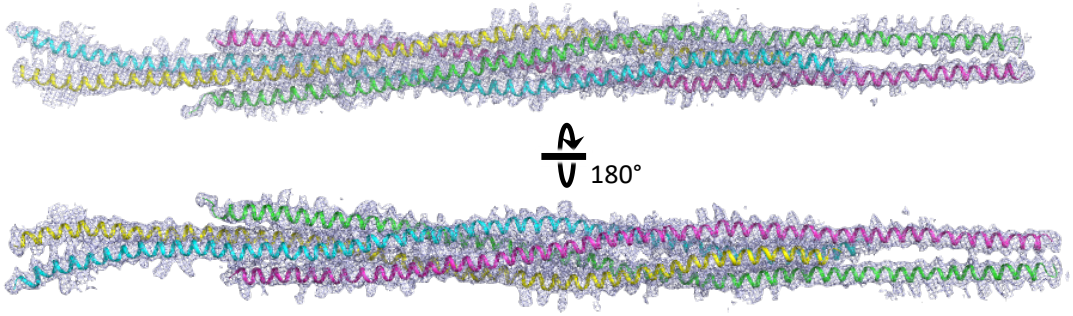

D **Views of the crystallographic packing arrangements of BASS-XL structure**

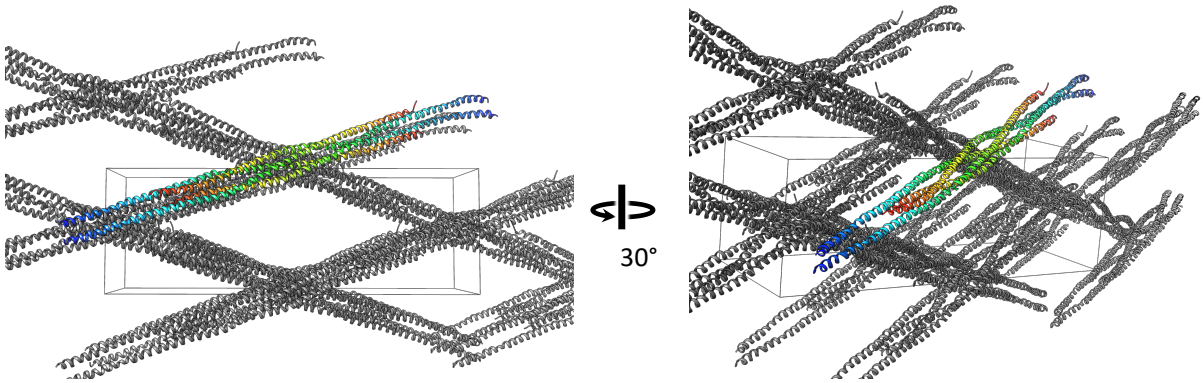

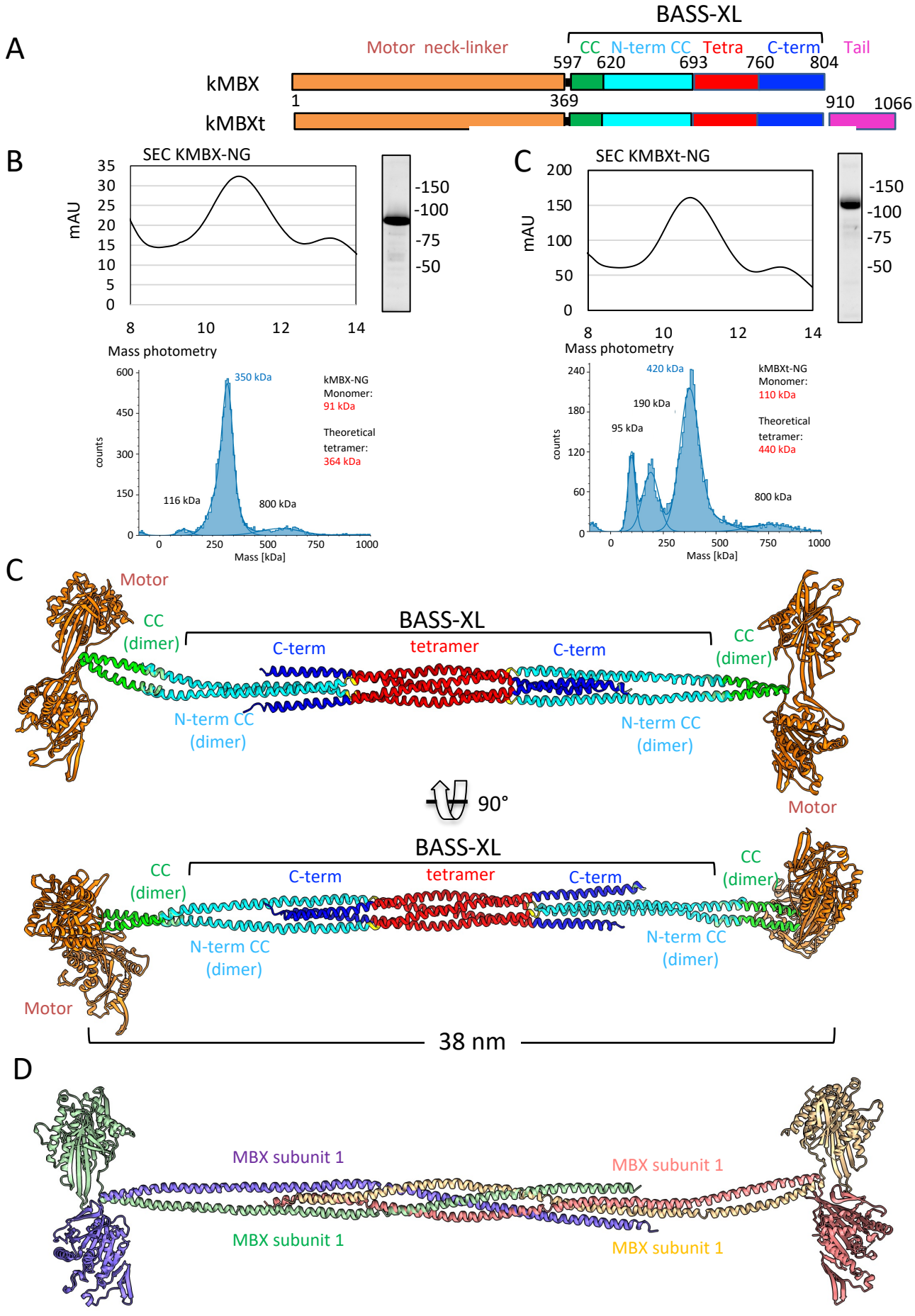
A
BASS-XL
Motor neck-linker
CC N-term CC Tetra C-term
Tail
597 620 693 760 804
kMBX
1 369 910 1066
kMBXt
B
SEC KMBX-NG
mAU
-150
-100
-75
-50
Mass photometry
350 kDa
kMBX-NG
Monomer:
91 kDa
Theoretical
tetramer:
364 kDa
116 kDa
800 kDa
counts
Mass [kDa]
C
SEC KMBXt-NG
mAU
Mass photometry
420 kDa
190 kDa
95 kDa
kMBXt-NG
Monomer:
110 kDa
Theoretical
tetramer:
440 kDa
800 kDa
counts
Mass [kDa]
C
Motor
CC
(dimer)
BASS-XL
C-term
tetramer
C-term
CC
(dimer)
N-term CC
(dimer)
N-term CC
(dimer)
Motor
90°
BASS-XL
CC
(dimer)
C-term
tetramer
C-term
CC
(dimer)
N-term CC
(dimer)
N-term CC
(dimer)
Motor
38 nm
D
MBX subunit 1
MBX subunit 1
MBX subunit 1
MBX subunit 1

Figure S3

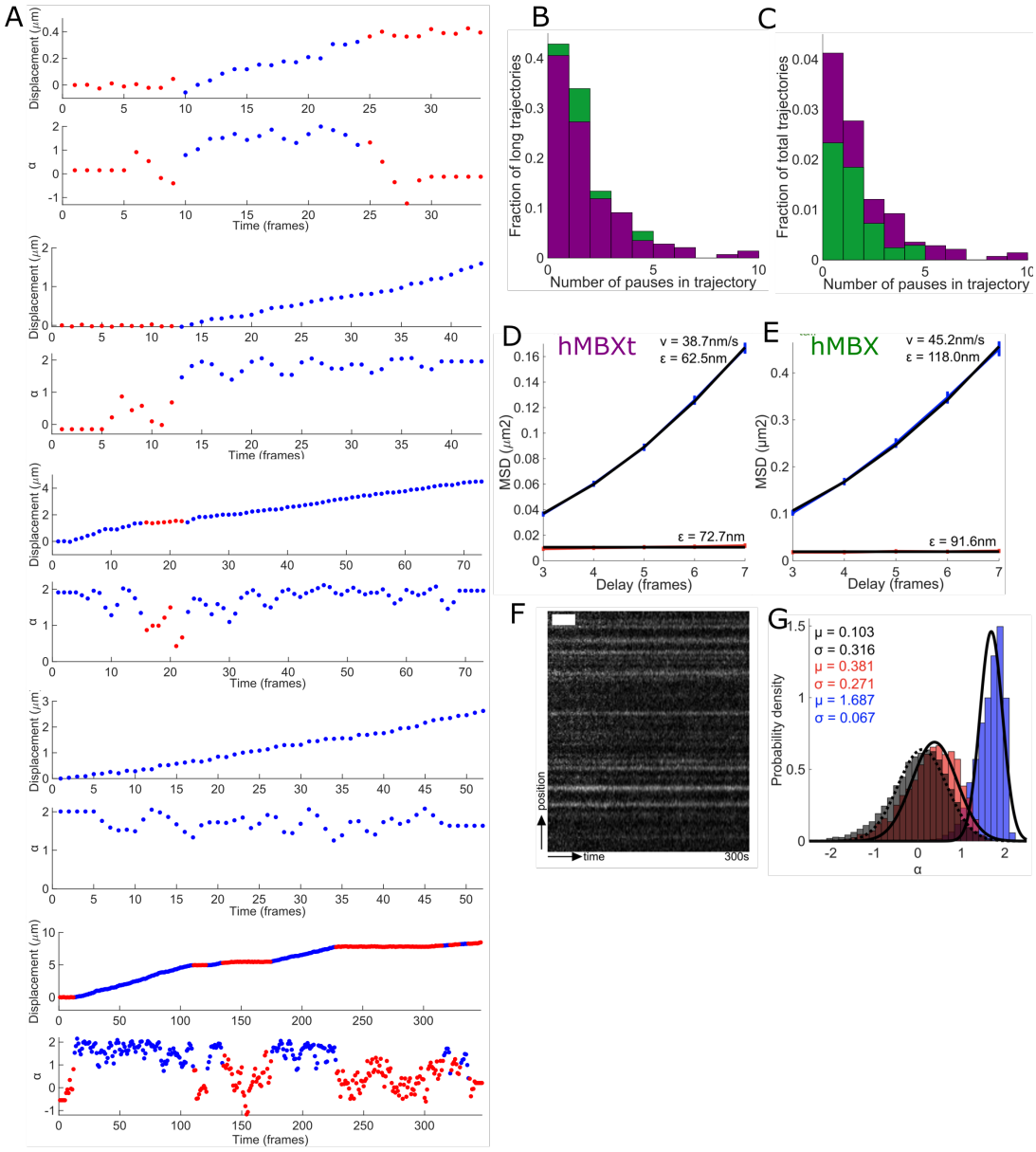
A
Displacement (μm)
α
Time (frames)
B
Fraction of long trajectories
Number of pauses in trajectory
C
Fraction of total trajectories
Number of pauses in trajectory
D
hMBXt
v = 38.7nm/s
ε = 62.5nm
ε = 72.7nm
MSD (μm2)
Delay (frames)
E
hMBX
v = 45.2nm/s
ε = 118.0nm
ε = 91.6nm
MSD (μm2)
Delay (frames)
F
position
time
300s
G
μ = 0.103
σ = 0.316
μ = 0.381
σ = 0.271
μ = 1.687
σ = 0.067
Probability density
α

A: Spot kMBXt motor identification and intensity analysis by trackmate plugin in ImageJ-Fiji

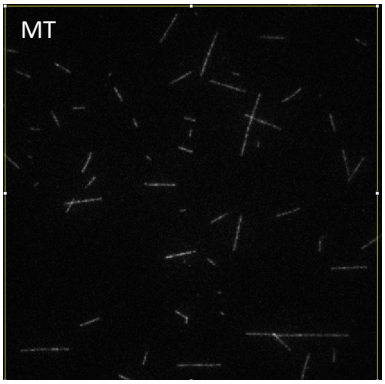

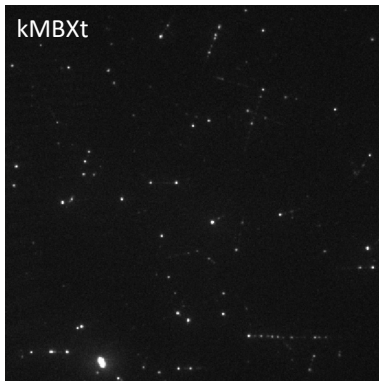

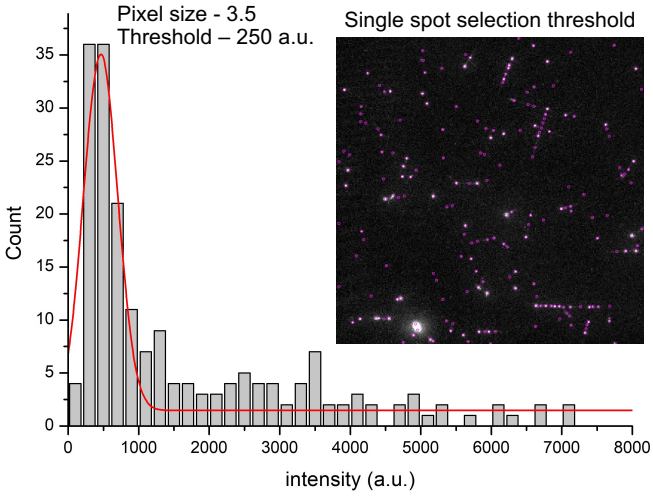

B: Kymographs for kMBXt clustering behavior at different KCl concentrations

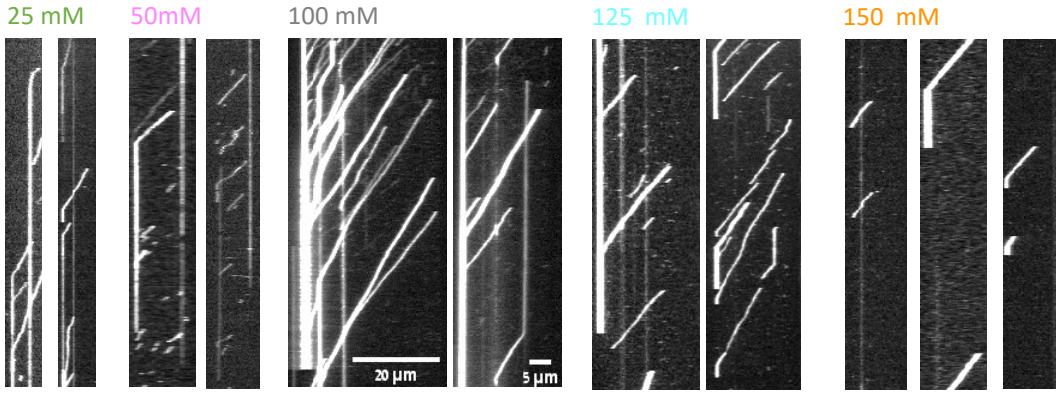

Types of merging events

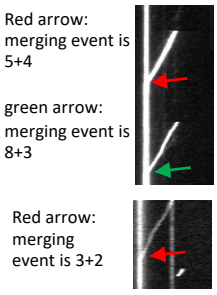

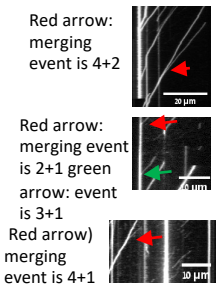

C: Velocity

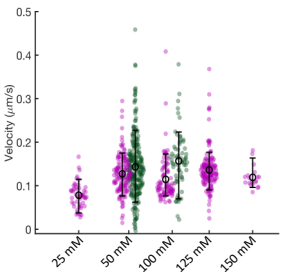

D : Run length

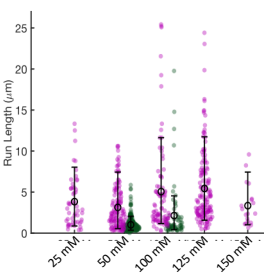

E : Run time

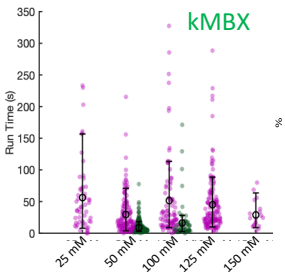

F: Types of clusters formed during motor merging events

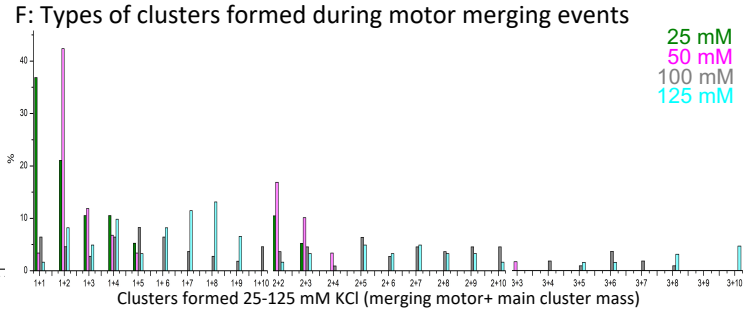

G: Per cluster state motility properties

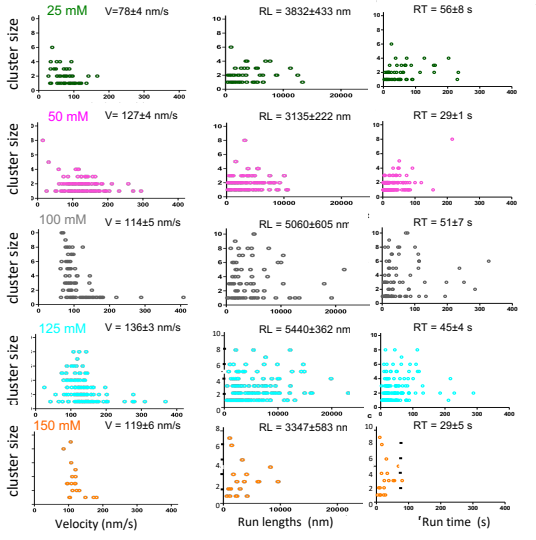

H

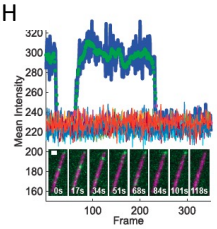

I

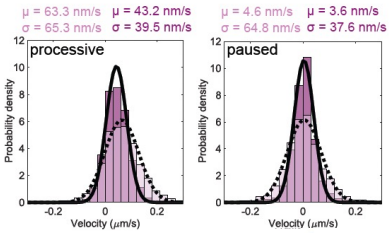

J

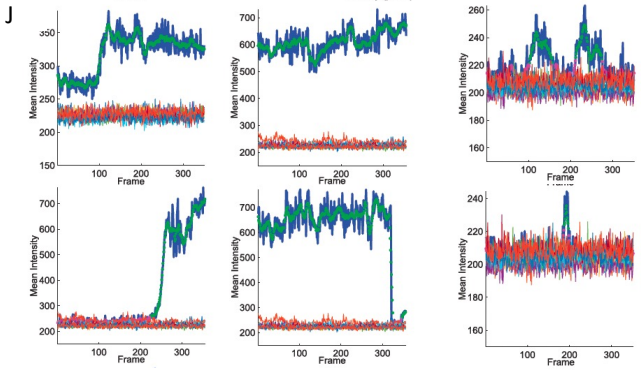

K

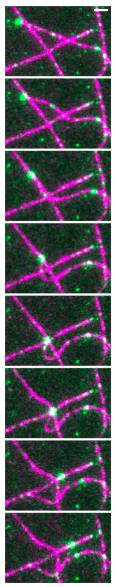

Figure S5

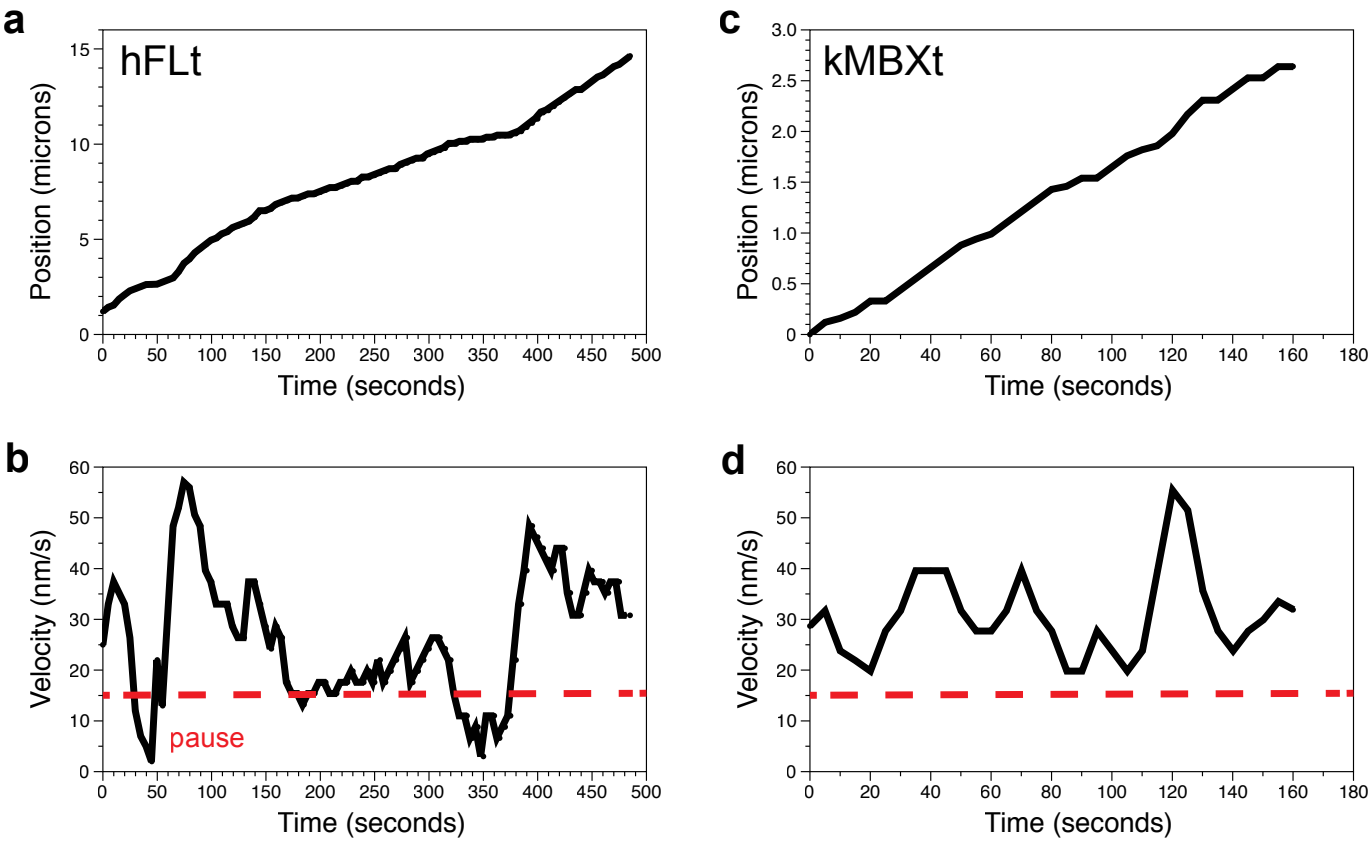
a
hFLt
Position (microns)
Time (seconds)
c
kMBXt
Position (microns)
Time (seconds)
b
Velocity (nm/s)
pause
Time (seconds)
d
Velocity (nm/s)
Time (seconds)